$BiVO_4$ Thin Films Design via Magnetron Sputtering for Water Treatment: Antimicrobial Activity, Photocatalytic Efficiency, and Toxicity Assessment

Guenther Carlos C. Viana [a], Marina Ratova [b], Artemis E. Dimopoulou [c], James Redfern [c], Kris O'Dowd [d], Peter J. Kelly [b], Suresh C. Pillai [d], and Camila C. Amorim [a*]

[a] Research Group on Environmental Application of Advanced Oxidation Processes (GruPOA), Federal University of Minas Gerais, Engineering School - Sanitary and Environmental Engineering Department, Av. Antônio Carlos 6627, 31270-901, Pampulha, Belo Horizonte, Brazil.

[b] Surface Engineering Group, Department of Engineering, Manchester Metropolitan University, Manchester M1 5GD, UK.

[c] Department of Natural Sciences, Faculty of Science & Engineering, Manchester Metropolitan University, M1 5GD, UK.

[d] Nanotechnology and Bio-Engineering Research Group & Health and Bio-medical Center, Atlantic Technological University, ATU Sligo, Ash Lane, Sligo, Ireland.

*camila@desa.ufmg.br

GRAPHICAL ABSTRACT

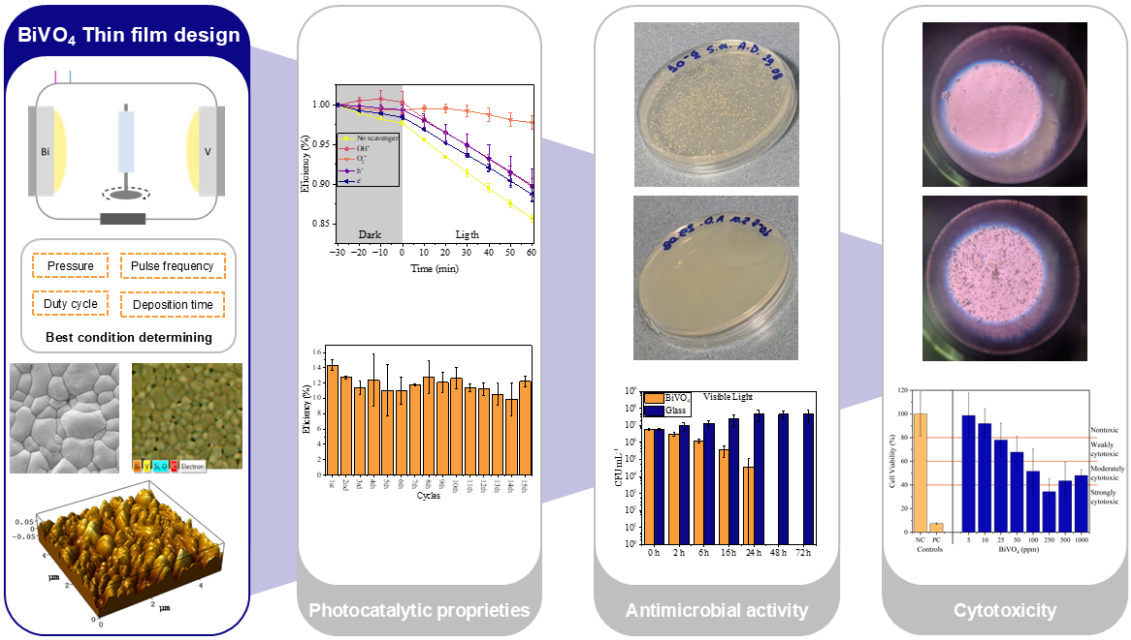

ABSTRACT

This paper investigates the production of bismuth vanadate ($BiVO_4$) thin film for photocatalytic water treatment, verifying the effect of operational parameters for $BiVO_4$ thin film production by magnetron sputtering. The samples were characterized and through photocatalytic assessment, the $BiVO_4$ optimal production condition was determined as being 4 mTorr of pressure, 100 kHz of pulse frequency, 90% of duty cycle, and 2 h of deposition time. The $BiVO_4$ antimicrobial proprieties were assessed following the British Standard ISO 27447:2009 with *E. coli*. Antimicrobial activity was observed under visible light, resulting in values under the detection limit (<LD) within 24h. The material showed activity in the dark, achieving values <LD within 48h. According to ISO 10993–5:2009, different cytotoxicity levels in humane intestinal cells were observed within the tested concentrations range. This antimicrobial activity is unprecedented, indicating a significant opportunity for advancement in disinfection and offering a safe alternative to conventional water treatment.

1. INTRODUCTION

The availability of sufficient and safe drinking water is a critical public health issue. One of the United Nations (UN) [1] Sustainable Development Goals is to ensure universal access to water and sanitation by 2030. Despite the improvements, access to safe drinking water remains a critical concern. In contrast, the World Health Organization (WHO) [2] estimates that globally, at least 2 billion people consume drinking water from sources with microbial contamination. This results in a considerable number of waterborne infections, causing diarrhea that kills almost one million people per year, primarily children under five years of age. In conventional water treatment, the microbial inactivation step is typically carried out using chlorination in the final stages of the treatment process [3]. Currently, alternatives are being sought due to the formation of by-products of chlorine disinfection that may have carcinogenic properties [4,5].

Heterogeneous photocatalysis is an Advanced Oxidation Process (AOP) that has been described as a suitable technology for enhancing safety in water treatment regarding disinfection [6–8]. However, this technology has faced several challenges, including

recovery, separation, and recycling of the photocatalyst, thus hindering large-scale application [9]. Another concern is the toxicity caused by the persistence of these particles in the treated matrix [10]. To avoid such issues, many researchers have adopted the strategy of immobilizing catalysts for use in photocatalytic processes [11–19]. Immobilized catalysts in thin films offer several advantages over suspended materials. These include reduced material usage, ease of recycling due to adhesion to a surface, less physical interference, and improved long-term performance [13].

Among the deposition techniques available, magnetron sputtering stands out as a relatively simple, versatile, and easily scalable vacuum-based method used to deposit various materials onto different supports. This physical deposition method (PDM) is advantageous in terms of its high productivity and ability to control particle size, when compared with chemical deposition methods (CDM) [13,20]. CDM usually has some disadvantages regarding high temperature and material loss in the production process, difficulties in scaling up production of films with large areas, and low photocatalytic efficiency [21,22]. In contrast, magnetron sputtering exhibits a high deposition rate at lower pressures and temperatures, resulting in the formation of resistant and uniform thickness coatings [23]. This process has undergone significant advancements in recent decades, becoming a preferred technique for many industrial processes. The driving force behind this development is the increasing demand for high-quality functional thin films in large scales across a wide range of sectors [20,24,25]. The technique's versatility is advantageous because the stoichiometry of the coating can be easily controlled by varying operational parameters and the chemical composition of the target [23].

Another limitation faced by applying heterogeneous photocatalysis as a water treatment technique is the applicability of the method under visible light. To address this challenge, bismuth-based oxides have been reported as promising materials due to their high photocatalytic activity resulting from enhanced charge transfer [26–32]. More specifically, bismuth vanadate ($BiVO_4$) has attracted significant interest due to its low band gap, non-toxicity, and corrosion resistance, resulting in excellent photocatalytic activity in the degradation of organic pollutants under visible light irradiation [33,34]. Having good chemical and photo stability, and a band gap of ~2.4, $BiVO_4$ became a significant strong candidate for solar energy harvesting [35,36]. However, some studies suggest that the photocatalytic behavior of pure $BiVO_4$ may need further enhancement

due to the rapid recombination of photo-induced carriers resulting from the narrow band gap value. Other limitations in the literature include low specific surface area, low carrier transfer, and low electron mobility [37]. Different morphology controls, doping with metallic and non-metallic elements, semiconductor coupling, and exposed reactive facets have been studied to address this [38–40].

The production of nanopowder $BiVO_4$ photocatalyst has been reported through various techniques [41–43]. However, in this form, the material exhibits the aforementioned disadvantages. In this respect, the design of thin film $BiVO_4$ materials for photocatalytic applications is one of the most compelling applications that can render the entire process more practical and economical. The synthesis of $BiVO_4$ thin films could be through RF sputtering [44], jet nebulizer spray pyrolysis equipment [45], cyclic voltammetry deposition, [46]. and reactive direct-current magnetron sputtering [47]. Some of these works used strategies of doping or heterojunction formation to achieve good photocatalytic activity with $BiVO_4$-based thin films [37,44,48–51]. However, these mentioned studies tested photocatalytic activity only for dye degradation and did not analyze the influence of production parameters on the film's performance.

Despite magnetron sputtering presenting numerous advantages and being an attractive technique for producing thin films of $BiVO_4$, limited literature explores this method for producing $BiVO_4$ thin films. On the other hand, this technique's utilization and optimization can potentially control film properties that impact photocatalytic activity, such as morphology, porosity, band gap, and crystalline structure [47]. Controlling these parameters is paramount in overcoming the limitations of $BiVO_4$ catalysts. Thus, the present work aims to address the observed gap and investigate how operational parameters for $BiVO_4$ thin film production by magnetron sputtering influence their chemical, physical, and optical properties and, consequently, their photocatalytic activity. Furthermore, this work aims to verify its antimicrobial and toxicological properties, describe its photocatalytic mechanism, and ultimately target applications in water treatment.

2. MATERIALS AND METHODS

2.1 Deposition conditions for $BiVO_4$ thin films

The thin films were deposited in a single step under a high vacuum in a Teer UDP 350 sputtering rig (Figure S1) onto 25 x 75 mm glass slides as substrates. Substrates were ultrasonically pre-cleaned in isopropanol (99%, Sigma-Aldrich) and then placed in the vacuum chamber. Two high purity (99.5%) metallic targets, Bismuth (Bi) and Vanadium (V) were bonded to copper backing plates and used as sputtering targets. Each target was mounted on a 300 mm X 100 mm type II unbalanced planar magnetron. The magnetrons were installed through the vacuum chamber walls surrounding the rotating substrate holder in a closed-field configuration. The distance between the target and the substrate was 50 mm for the deposition of all samples. The argon flow was kept constant at 40 sccm and the oxygen flow at 20 sccm, and the time-averaged power applied to the magnetrons were 50 W to Bi and 800 W to V. The magnetrons were powered by a dual-channel Advanced Energy Pinnacle Plus source operating in pulsed DC mode.

A Design of Experiments Taguchi type L9 array was used to determine the optimum deposition conditions to produce efficient $BiVO_4$ photocatalytic thin films. This design has been extensively utilized for this purpose in numerous research domains [52]. Methodology for reactive sputter deposition of bismuth vanadate has been previously developed by the authors, however no systematic investigation of deposition parameters on properties of bismuth vanadate coatings. The experimental design utilized in the present work involved the variation of several parameters and levels, including pressure (4, 6, and 8 mTorr), pulse frequency (100, 200, and 300 kHz), duty cycle (60, 75, and 90 %), and deposition time (0.5, 1.0, and 2.0 h). The deposition parameters varied have been earlier demonstrated to have a significant effect on morphological and phase properties of the materials [20]. The experimental design yielded nine distinct experimental conditions, which were tested to produce $BiVO_4$ thin films, identified as BV1, BV2, BV3, BV4, BV5, BV6, BV7, BV8, and BV9. Each experimental condition can be seen in Table S1. All the coatings were annealed at 500°C for 1 h in air with a heating ramp of 10°C min^{-1} and then allowed to cool gradually to avoid thermal stress formation. The results of the Taguchi L9 array were analyzed using Minitab 17 statistical software.

2.2 Characterization of the $BiVO_4$ thin films

The thickness of the samples was measured by covering a portion of the microscope glass slide with Kapton tape before deposition. The height of the resulting artificial step formed when the tape was removed after deposition was then measured using a Profilm3D interferometer from Filmetrics, with a magnification of ×50. The optical absorbance of the samples was measured, and the optical band gap of $BiVO_4$ was estimated using the Tauc plot method [53]. The crystallography of the thin films was studied with X-ray diffraction (XRD) (Panalytical Xpert powder with CuKa1 radiation at 0.154 nm in grazing incidence mode at 3° over a scan range from 20° to 70° 2θ; the accelerating voltage and applied current were 40 kV and 30 mA, respectively). The thin films' elemental composition was determined with SEM/EDX (EDAX Trident, Edax Co. installed on a Zeiss Supra 40 VP-FEG-SEM). Surface morphology, roughness, and area were conducted using a Horiba XPlora Plus atomic force microscopy (AFM) system. The catalyst load per area was estimated by weighing the coated and uncoated glass slides. The transmission electron microscopy (TEM) micrographs were obtained using a FEI Titan Themis FEG STEM; prior to that, a lamella was extracted from the bulk of the sample using an FEI Helios G4CX FIB-SEM.

2.3 $BiVO_4$ thin films photocatalytic activity assessment

The photocatalytic activity of all $BiVO_4$ thin films produced was evaluated using a methylene blue (MB) degradation test, measuring the absorbance of the solution at 664 nm. The initial concentration of the testing solution was 2 μmol L^{-1}. The photocatalytic activity tests were performed using a visible light source with a 60 W daylight bulb. The emission spectrum of the irradiance source is in Figure S2; the integrated irradiance value in the 400–800 nm wavelength range was 190 W m^{-2}. For each condition from the experimental design, a 25 x 15 mm^2 sample of $BiVO_4$ thin film was tested. Before the photocatalytic tests, all $BiVO_4$ thin film samples were immersed in MB solution (the same concentration as the testing solution) and kept in the dark at room temperature (25°C) for 1 h, with continuous magnetic stirring (≈150 RPM), to reach the adsorption-desorption equilibrium. After that, the photocatalytic tests were conducted for 1 h for all test runs. A reference test for MB photolysis was also carried out under the same irradiation source but in the absence of a photocatalyst.

Through the results obtained in the photocatalytic tests, the optimum conditions to produce $BiVO_4$ thin films were defined. Subsequently, the optimal $BiVO_4$ thin film was submitted to recycling tests for repeated MB degradation cycles. Furthermore, to describe the photo-degradation reaction mechanism of the optimal $BiVO_4$ thin film, photocatalytic tests were conducted in the same conditions previously described, in the presence of different scavengers. The following trapping agents were employed: isopropanol [54–56] for •OH, 4-hydroxy TEMPO [56,57] for $O_2^{\bullet-}$, sodium oxalate [58,59] for h^+ and sodium nitrate [60] for e^-. The concentration of each scavenger was 7 mmol L^{-1} [31].

2.4 $BiVO_4$ thin film antimicrobial activity assessment

To test the antimicrobial activity of $BiVO_4$ thin films a slight adaptation of the British Standard (BS) ISO 27447:2009 was used. *Escherichia coli* (*E. coli*) NCTC 9001 was stored in glycerol stock at −80°C. For experimental work, the microorganism was subcultured from the stock onto nutrient agar (NA) (BD, Sparks, MD), and incubated overnight at 37°C. For testing antimicrobial potential, 2–4 colonies of *E. coli* were inoculated into 10 mL of 1/500 nutrient broth (NB, Oxoid, Basingstoke) and the solution was vortexed for 60 s. Once the solution has reached 0.1 optical density at 600 nm (Jenway 6305 Spectrophotometer, UK), two 10-fold dilutions were performed using 1/500 Nutrient Broth resulting in a standardized bacterial suspension of $2.0 \pm 0.7 \times 10^6$ CFU mL^{-1}.

All solutions and equipment used in this test were either sterile from the manufacturer or autoclaved for 20 min at 121°C. A paper filter was placed at the bottom of a sterile Petri dish, and 5 mL of sterile distilled water was added to ensure high humidity during the experiment. Sterile glass beads were placed on top of the wet filter paper to avoid direct contact between the test piece and the water. The uncoated or coated glass samples with $BiVO_4$ thin films were placed on top of the glass beads in the Petri dishes. 25 µL of standardized bacterial suspension was pipetted on each test piece, with a sterile polystyrene film laid on top to ensure even spread across the surface. Then the Petri dish lid was placed and sealed with parafilm for moisture conservation. This sealing with parafilm was the modification made to the BS ISO 27447:2009 due to the observation in the preliminary tests, which showed a visible loss of moisture throughout the test. Both samples, uncoated and glass coated with a $BiVO_4$ thin film, were tested under the visible light source and in the dark for 0, 2, 6, 16, 24, 48, and 72 h. For the samples treated with

visible light, the light source described in topic 2.3 was used. The experiments for each condition, sample, and time were repeated in triplicate. After its specific time, each sample was immediately washed out into a stomacher bag with 10 mL of soybean-casein digest broth with lecithin and polysorbate 80 (SCDLP), as described in the BS ISO 27447:2009. Following 10-fold dilutions up to 10^{-6} in physiological saline, this washout solution was used to determine the number of viable cells via enumeration of colony forming units (CFU). For each series of dilutions, 100 µL was plated in duplicate in Petri dishes with nutrient agar. The plates were incubated overnight at 37 °C. Finally, colony numbers were counted in the series of Petri dishes with colony numbers between 30-300. The whole experiment was repeated three times to ensure reproducibility.

2.5 $BiVO_4$ cytotoxicity assessment

All materials used were of analytical grade. Methanol (CH_3OH) was purchased from Analab. CACO-2 cell line humane intestinal cells were purchased from Sigma. DMEM medium glucose (Dulbecco's Modified Eagle Medium)-High Glucose, Fetal Bovine Serum (FBS), catalase, and Dulbecco's Phosphate Buffered Saline (PBS) were purchased from GE Healthcare. Trypsin, 0.25% (1x), with 2.5 g porcine in HBSS, Trypan blue, and Thiazolyl blue tetrazolium bromide 98% (MTT) were purchased from Fisher Scientific. Penicillin Streptomycin Sol 100 mL, L-Glutamine 200 mm 100 mL, and DMSO, LC-MC Grade were purchased from biosciences. T75 and T25Tissue Culture Treated Flasks (vented caps), 10/25/50 mL Serological Pipette (sterile), individually wrapped, and 1/0.2/0.01 mL pipette tips were purchased from Starstedt. 96 well plates from MSC. Oasis HLB 5 cc Glass, 200 mg cartridges from waters. 4 mL screw neck vials were obtained from VWR. IST 20 L VacMaster was obtained from the I.T. stores. A BMG Labteck FLUOstar Omega microplate reader was supplied by I.T. technical staff.

CACO-2 cells were maintained in DMEM medium containing 20% fetal bovine serum and 1% pen/strep. Before analysis, a 96 well plate was seeded with a cell concentration of 7500 cell/well with a volume of 100 µL. After allowing the cells to attach for 24 h the media was removed and 100 µL of controls were added; a blank (media), a negative control (media + 1% (v/v) DMSO), and a positive control (media + 10% (v/v) DMSO).

To assess the cytotoxicity of the material, the $BiVO_4$ thin films produced in the best condition were mechanically peeled from the substrate by friction with a spatula, and the

powder obtained was used for the tests. Seven concentrations of material were added at 5, 25, 50, 100, 250, 500, 1000 mg L^{-1}. All were exposed for 24 h, after which the media was removed, and the wells were washed with 100 µL of PBS. 100 µL of fresh media and 10 µL of MTT reagent was added and the plates were incubated for at least 4 h. After incubation, all contents were removed from the wells and 100 µL of DMSO was added. The absorbance was read at 580 nm on a BMG Labteck FLUOstar Omega microplate reader (Ortenberg, Germany) with the shake plate feature on and analyzed for 15 min. Comparing the absorbance of the control with treated cells can be used to calculate the percentage viability of the treated cells. Viability of 40% or below is considered strongly cytotoxic, 40–60% moderately cytotoxic, 60–80% weakly cytotoxic, and above 80% is seen to be nontoxic as per ISO 10993–5.

3 RESULTS AND DISCUSSION

3.1 Deposition conditions assay for the $BiVO_4$ thin films

3.1.1 Characterization of $BiVO_4$ thin film

After producing films at each set of array conditions, the resulting $BiVO_4$ thin films were characterized, and the influence of each designed parameter was assessed. Deposition time had a strong influence on the thickness of the thin films, as expected (Table S1, Figure S3). Pressure and pulse frequency also had a linear positive effect on the deposition rate, but with less influence when compared to the deposition time. Regarding the duty cycle, the lowest tested value resulted in thicker films (Figure S3). According to [58], the peak current and power density are higher at low duty cycles. This condition leads to a higher ionization rate of the gases in the discharge increasing the plasma density and the deposition rate [62]. It is crucial to underscore that deposition time is the dominant factor influencing film thickness, with the other parameters exerting a secondary influence.

The XRD patterns (Figure 1) show that the different experimental design conditions resulted in varying peak intensities. The data from the crystallographic database indicates that the XRD patterns corresponded mainly to the $BiVO_4$ monoclinic phase (JCPDS 01-083-1699), with very few tetragonal phases (JCPDS 00-014-0133). This response indicates that the factors, within the applied levels, predominantly result in the formation of the monoclinic phase of $BiVO_4$. The samples were found to be predominantly

crystalline, with no amorphous components, as evidenced by their flat, low-noise baseline. Furthermore, the intensity of the peaks indicated that sample BV3 exhibited a higher degree of crystallinity compared to the others. In addition, the ratio of exposed crystal faces of $BiVO_4$ varies between the analyzed conditions. Among them, the ratio of (121) ($2\theta = 28.8°$) to (040) ($2\theta = 30.5°$) crystal faces of film BV3 is the highest, indicating that this production condition is conducive to the exposure of (121) crystal faces, which have a high refractive index [63]. This process can facilitate accelerated oxidation kinetics, which is beneficial for enhancing the catalytic efficacy [64]. Such desirable properties were expected to be found at the lower tested pressures (2 mTorr); higher pressures result in a lower deposition rate, thereby reducing crystal growth [65,66]. This behavior was indeed observed in the present study. Sample BV9, produced at a higher pressure (8 mTorr), exhibited markedly low peaks, indicating reduced crystallinity. Similarly, the deposition time substantially impacts this film's propriety [67]. The maximum and minimum levels for this factor were employed in the production of BV3 and BV9 (2.0 and 0.5 h, respectively), thereby influencing the resulting crystallinity degrees. High crystallinity is advantageous as it positively influences the photocatalytic performance of semimetals [13,68,69].

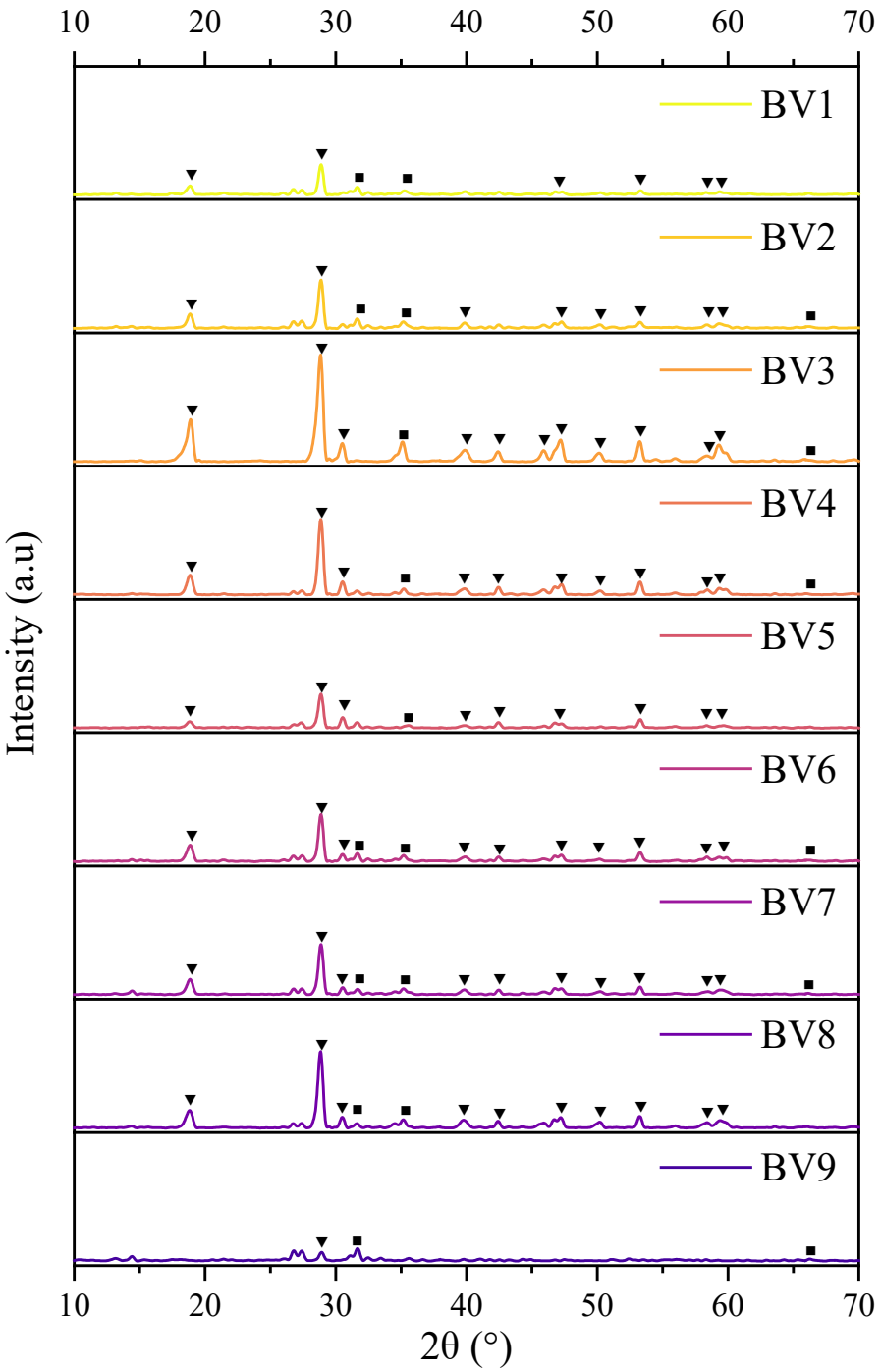

Figure 1 XRD patterns of $BiVO_4$ thin films resulting from L9 Taguchi design and annealed at 500°C for 1 h in air with a heating ramp of 10°C min^{-1}.

The produced thin film demonstrated the desired composition, and a homogeneous spatial distribution of the compounds Bi, V, and O. The results for the main components - Bi, V, and O - can be seen in graphs constructed with EDX data (Figure S4). Given that the

objective was to produce $BiVO_4$, the atomic proportion should be 1:1:4 for Bi:V:O. In some conditions, the atomic percentage of O was higher than expected. It was particularly prevalent in the case of very thin films, and the high oxygen contents may be attributable to the substrate. Values of V seems to be quite low compared to values of Bi. However, applying the Mann-Whitney statistical test for each sample, the difference between the atomic percentage of Bi and V are not significantly different ($\alpha = 0.05$), demonstrating a consistent result to those expected for $BiVO_4$. Accessing the ratio between Bi and V and comparing the nine produced samples trough Kruskal-Wallis's test followed by Dunn's test, the difference between them is not statistically significant ($\alpha = 0.05$) as well. It is noteworthy that EDX and XRD results show that the material produced under different conditions is, in fact, $BiVO_4$. However, the impact of the differences between the samples resulted from the experimental design will become more evident in the photocatalytic activity of each produced thin film.

The material light absorbance assessed for the band gap calculations resulted in a high transmission in the visible range (Figure S5). This characteristic is desirable and indicates that visible light can activate the material and be applied in water treatment processes with solar radiation. The assessed band gap values (Table S1), calculated through the Tauc plot method (Figure S6), are similar to those reported in the literature for $BiVO_4$ monoclinic phase ~2.4 eV [37,70]. The results obtained range from 2.29 to 2.47 eV (Table S1). Analyzing the main effect plots for the band gap energy, the deposition time has the most decisive influence, which is negative and linear (Figure S7). The duty cycle also had a significant positive effect on the resulting band gap value (Figure S7). A low significance was observed with a non-linear effect when evaluating the pressure factor. Regarding pulse frequency, a negative and linear effect was observed, but with low significance (Figure S7). The low significance of pressure and pulse frequency being analyzed individually - which is possible through Taguchi experimental design - is to be expected for a complex variable such as these. In order to gain a deeper understanding of the effect of these factors, it is necessary to apply an experimental design that can model the interactions between the analyzed factors and their non-linearities.

A detailed examination of the SEM images at 50000x magnification of the produced conditions reveals significant variations between the different production conditions. The samples subjected to a longer deposition time (BV2, BV4, and BV8) exhibited a denser coating with a larger crystalline structure, greater homogeneity, porosity, and higher grain

size (Figure 2). These findings underscore the intricate relationship between deposition time and the crystalline structure of magnetron-sputtered thin films. As the deposition time increases, it is observed that there is a notable increase in crystal growth. This phenomenon can be attributed to the prolonged interaction between the sputtered atoms and the substrate surface, which allows for enhanced atomic rearrangement and crystalline growth [23,62]. Grag et al. [67] highlighted that thin films with larger grains are more efficient photocatalysts. This phenomenon can be attributed to the increased roughness and surface area, which leads to enhanced interaction with the contaminants.

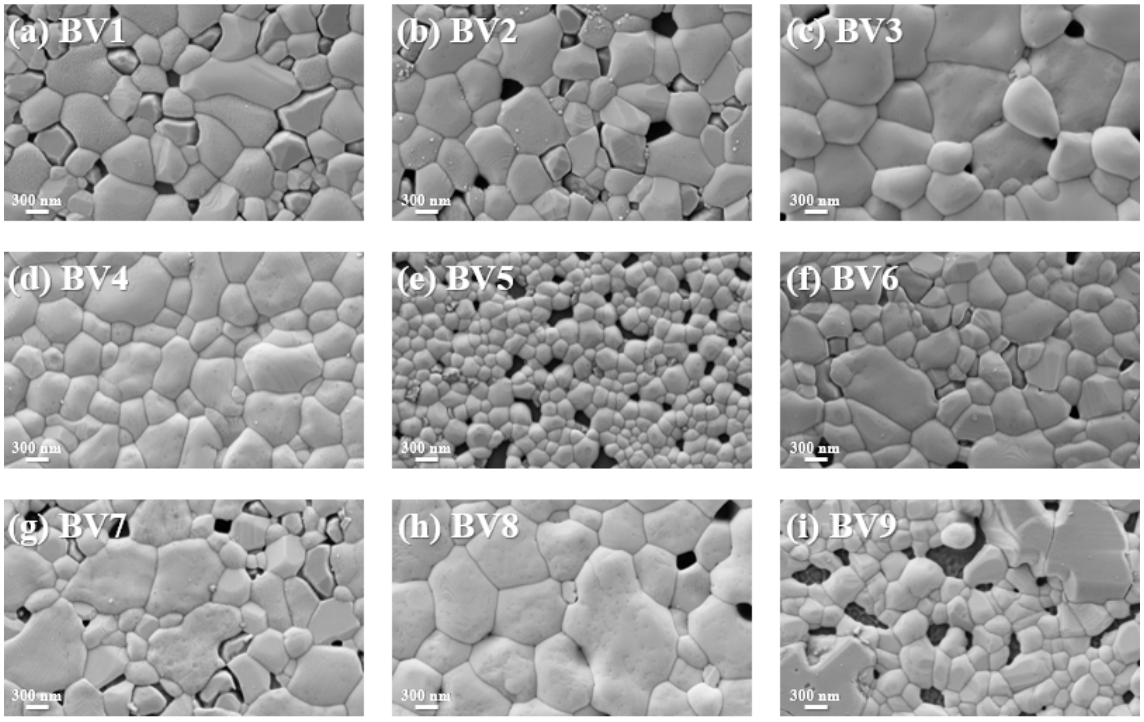

Figure 2. SEM 50.000x magnification of the samples resulting from L9 Taguchi design for $BiVO_4$ thin film production: (a) BV1, (b) BV2, (c) BV3, (d) BV4, (e) BV5, (f) BV6, (g) BV7, (h) BV8, and (i) BV9.

The impact of the growth parameters on the characteristics of the film is more clearly demonstrated through the AFM analysis performed on all samples resulting from the L9 Taguchi design (Figure 3). The surface roughness (Ra) data can be found in Table S1, and the main effect plot for this response is presented in Figure S8. This data showed that the factors with the greatest influence on Ra were pressure and deposition time. The deposition time exhibited a positive and linear effect, resulting in elevated values of Ra for high values of this factor. Conversely, a lower pressure has been observed to yield a higher Ra value. As elaborated in the XRD discussion, these conditions (low pressure and

high deposition time) result in elevated deposition rates, consequently yielding films with rougher surfaces. Similarly, Zang et al [71] findings indicate that an increase in sputtering pressure results in the formation of more surface cracks, smaller grain sizes, and a reduction in the roughness of the film.

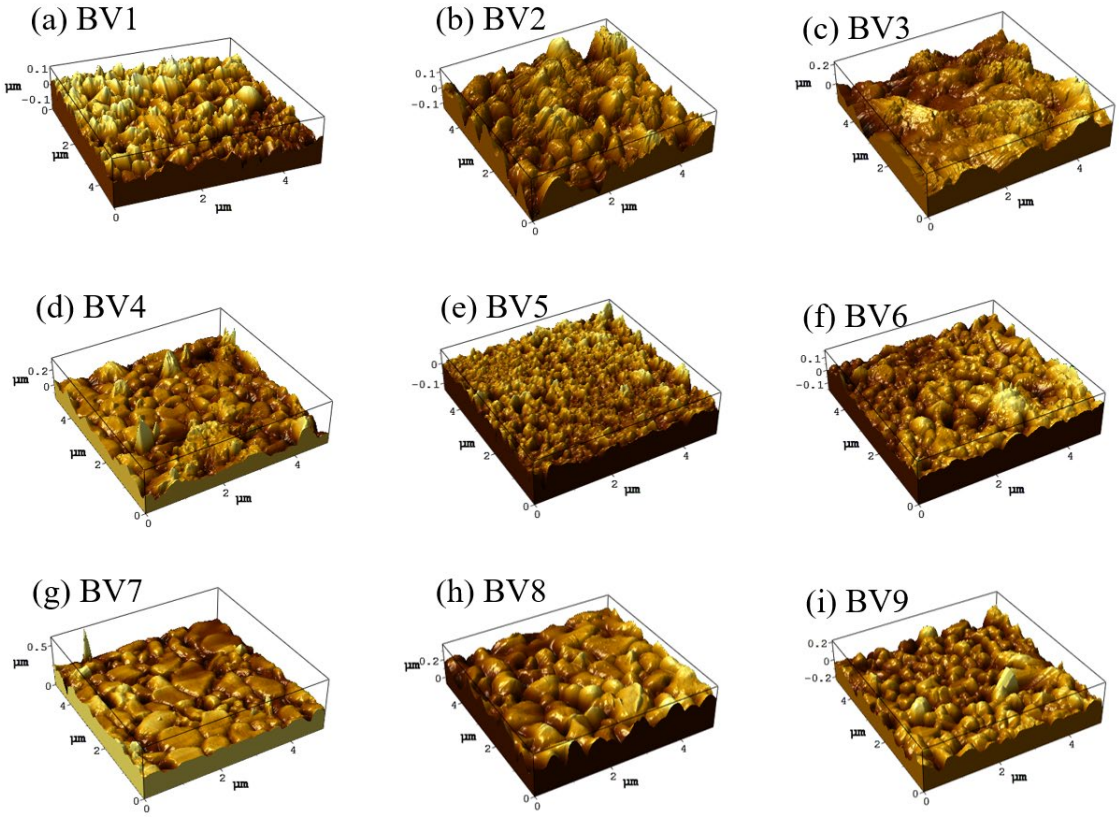

Figure 3. Three-dimensional AFM images of the samples resulting from L9 Taguchi design for BiVO4 thin film production: (a) BV1, (b) BV2, (c) BV3, (d) BV4, (e) BV5, (f) BV6, (g) BV7, (h) BV8, and (i) BV9.

3.1.2 Photocatalytic activity assessment of $BiVO_4$ thin films

Respecting photocatalytic activity, different outcomes result from each sample, ranging from 6.0 (BV1) to 19 % (BV4) MB degradation efficiency (Figure 4a). The pseudo-first-order kinetic constants varied widely but by the same order of magnitude (10^{-5}) (Figure 4b). In a study published by Grao et al. [65], a $Bi_{12}TiO_{20}/Bi_4Ti_3O_{12}$ composite catalyst was produced via magnetron sputtering, resulting in a k value of 7.76×10^{-5} s^{-1} for MB degradation. Similarly, Ratova et al. [30] produced bismuth oxide and bismuth tungstate via magnetron sputtering, achieving k values of 3.75×10^{-5} and 3.09×10^{-5} s^{-1},

respectively. In this context, the outcomes of this study are comparable to those of other bismuth-based compounds produced using the same technique.

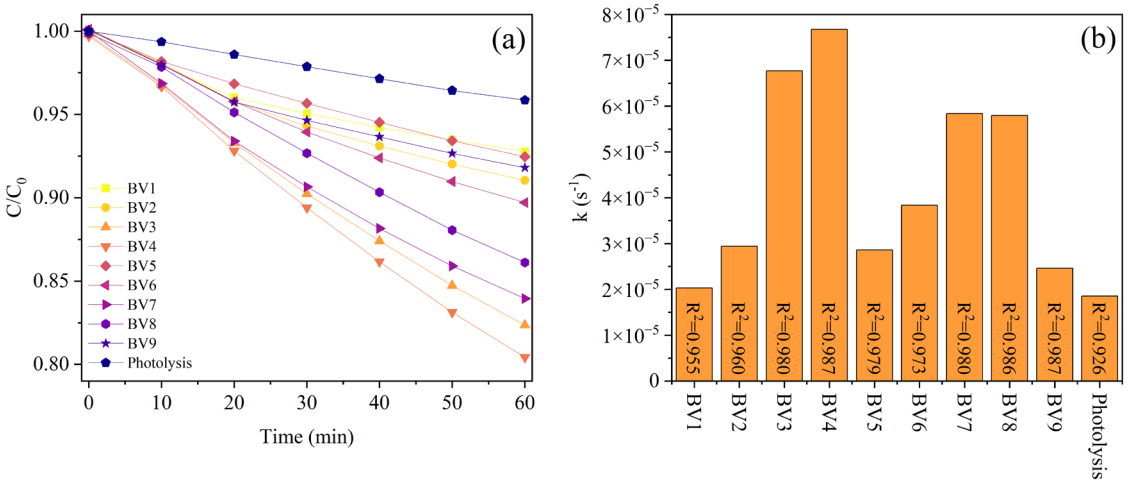

Figure 4. (a) Degradation over time and (b) pseudo-second-order kinetic constants performed by each sample resulting from L9 Taguchi design for $BiVO_4$ thin film production.

A subsequent cross-checking of information regarding the characterization of thin films and their photocatalytic activity revealed several noteworthy aspects. The materials that demonstrated lower degrees of crystallinity by XRD analysis (BV1 and BV9) were the samples with lower activity. Likewise, the sample with lower Ra (BV5, see Table S1) resulted in lower degradation rates (Figure 4). A strong crystallinity and large surface roughness are desirable characteristics that are extensively related to the photocatalytic efficiency of thin films [67,73,74].

Analyzing the main effect plot for photocatalytic degradation efficiency, a positive and linear influence of duty cycle and deposition time can be observed (Figure S9). This result corroborates the answers previously discussed, as higher levels of these factors resulted in a greater band gap and consequently more consistent photocatalytic activity. This greater band gap value comes from a bigger distance between the conduction and valence bands, resulting in less recombination of the charges formed on the surface of the thin film after its photoactivation. On the other hand, there is a negative linear influence for pressure. The frequency factor did not show linearity, but the results indicate better photocatalytic activity associated with the lowest frequency.

Thus, after studying the physical, chemical, optical, and photocatalytic properties of the films produced under different conditions, the best conditions for $BiVO_4$ thin film production were determined: 4 mTorr pressure, 100 kHz pulse frequency, 90% duty cycle, and 2 hours deposition time. This condition indicates the highest photocatalytic activity amongst the tested samples, as seen in the photocatalysis main effect plot (Figure S9).

3.2 Optimal $BiVO_4$ thin film assessment

3.2.1 Optimal $BiVO_4$ thin film characterization

The optimal $BiVO_4$ thin film was observed to have a 566 ± 9 nm thickness. This film showed significant transmission in the visible wavelength range (Figure S10a). Using this result to calculate the band gap through the Tauc plot method achieved a value of 2.45 eV (Figure S10b). The surface morphology of the optimal $BiVO_4$ thin film was studied with SEM and AFM; the micrographs are presented in Figure 5a-e. The surface roughness (Ra) was 41.69 nm. The coating exhibited well-defined crystals with good coverage and homogeneity.

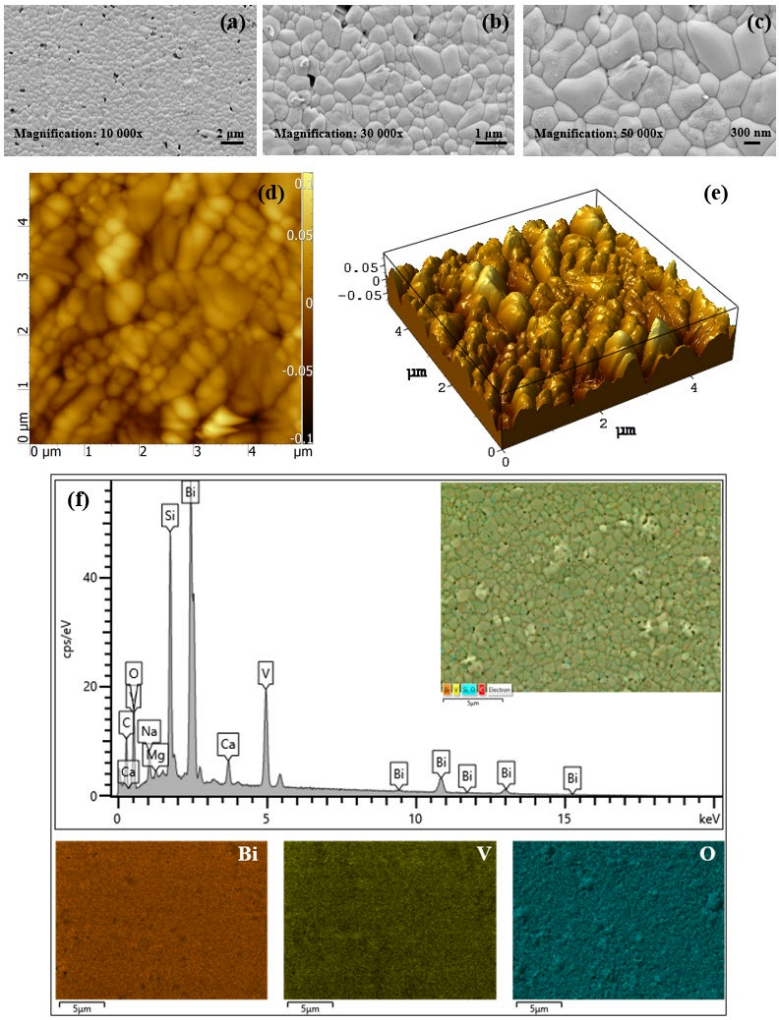

Figure 5. SEM micrographs in different magnifications: (a) 10 000x; (b) 30 000x; and (c) 50 000x, and AFM micrographs (d) 2D and (e) 3D of optimal $BiVO_4$ thin film, produced under the best conditions resulted from the Taguchi L9 method. (f) EDX pattern, mapping of the sample and the main components, bismuth (Bi), vanadium (V), and oxygen (O), for the samples of optimal $BiVO_4$ thin film.

The XRD patterns for the optimal $BiVO_4$ thin film exhibited a high degree of crystallinity, as evidenced by the intense peaks observed (Figure S11). The detected peaks primarily correspond to the $BiVO_4$ monoclinic phase (JCPDS 01-083-1699), demonstrating the superiority of this phase as well as the samples from the L9 Taguchi design. It is important to highlight that the monoclinic phase has higher photocatalytic performance under visible light due to the lone pair distortion of Bi 6s orbital in the $BiVO_4$ catalyst. The distinct overlap of the O 2p and Bi 6s orbitals in the valence band (VB) is advantageous for the mobility of photo-generated charge carriers, resulting in enhanced photocatalytic

activity [36,40,70,75–78]. The EDX results confirm the composition observed in the XRD patterns, and a well distributed composition of the main components (Figure 5f).

3.2.2 Optimal $BiVO_4$ thin film photocatalytic recycling test

In the optimal condition, the photocatalytic property of the $BiVO_4$ thin film was tested and yielded a kinetic constant (k) equal to $3.65x10^{-5}$ s^{-1}. This optimal $BiVO_4$ thin film was tested for 15 consecutive cycles without a significant efficiency reduction (Figure S12), as assessed using Kruskal-Wallis's test followed by Dunn's test ($\alpha = 0.05$). It is worth noting that no thermal treatment was carried out in the film in between each test cycle. Grao et al. [65] testing $Bi_{12}TiO_{20}/Bi_4Ti_3O_{12}$ composite catalyst via magnetron sputtering obtained stability during fifteen cycles as well. Yoon et al. [70] produced a $BiVO_4$ via the dip-coating method and tested its recyclability until the 25th cycle, achieving stability only until the 5th cycle. Lopes et al. [71] produced carbon-supported $BiVO_4$ using a chemical bath deposition method but were unable to achieve stability. The tests were conducted until the 3rd cycle and the efficiency reduced drastically. The fact that optimal $BiVO_4$ thin film, produced in this investigation, maintained its efficiency up to the 15th cycle confirms the quality of the thin film produced using the optimized conditions determined for magnetron sputtering. This characteristic is of the utmost importance to enable the application of photocatalytic processes in water treatment on a larger scale.

3.2.3 Photocatalytic degradation mechanism investigation

Through the reaction in the presence of different trapping agents, the mechanism behind the photocatalytic degradation of pollutants was assessed Figure 6a. The reactions in the presence of 4 hydroxy-TEMPO significantly reduced the photocatalyst's activity, indicating that the superoxide radicals ($O_2^{-\bullet}$) are the main oxidizing species acting in the reaction mechanism. It was observed in the literature that in the study of other $BiVO_4$-based catalysts, the $O_2^{-\bullet}$ was the most active species [27,81,82]. These radicals are formed by the reaction between the oxygen present in the medium and the electrons (e^-) formed in the conduction band (CB) [8,83]. There was an efficiency reduction in the reactions in the presence of isopropanol and sodium oxalate, indicating the participation of hydroxyl radical ($OH^\bullet$) and holes (h^+) in the reaction mechanism, but to a lesser extent.

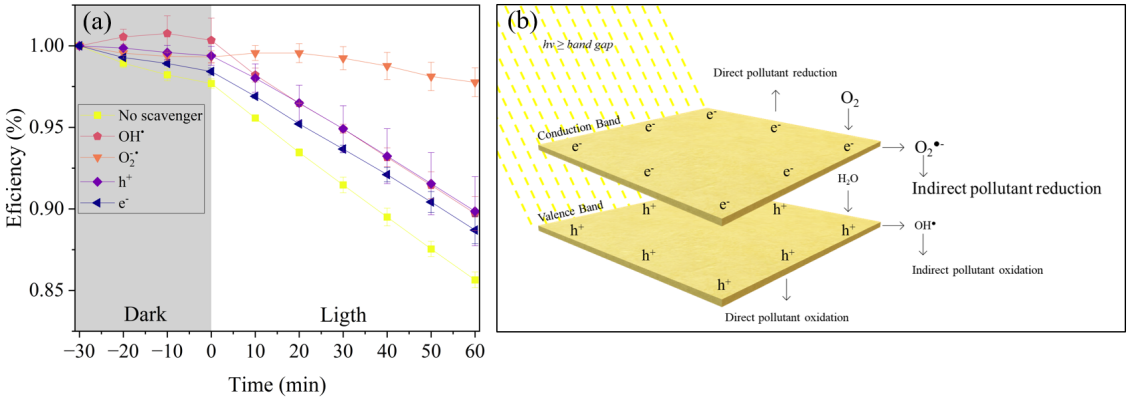

Figure 6. (a) MB degradation by the optimal $BiVO_4$ thin film under visible light irradiation in the presence of scavengers, isopropanol for $OH^{\bullet}$, 4-hydroxy TEMPO for $O_2^{\bullet-}$, sodium oxalate for h^+, and sodium nitrate for e^-. (b) Schematic of proposed photocatalysis mechanism in $BiVO_4$ thin film.

This analysis indicates that the $BiVO_4$ photocatalytic thin film activation process results in the transfer of e^- from the valence band (VB) to the CB, thereby generating electron-hole pairs (e^-/h^+). The dissolved oxygen in the media reacts with the e^- formed in the CB, forming $O_2^{-\bullet}$, which are reductive species, leading to indirect pollutant reduction. This proved to be the primary mechanism responsible for the efficiency of the process as previously described. The pollutant reacts directly with the e^- in the CB, resulting in a direct reduction. In the VB, the holes (h^+) formed react with the pollutant, leading to direct oxidation. In the same way, water (H_2O) molecules react with h^+ getting hydroxyl radicals ($OH^{\bullet}$) which leads to indirect pollutant oxidation. This proposed mechanism for the photocatalytic degradation of pollutants by $BiVO_4$ thin films is illustrated in Figure 6b.

3.3 Optimal $BiVO_4$ thin film antimicrobial activity assessment

To assess the antimicrobial propriety of the optimal $BiVO_4$ thin film, it was tested under visible light. To ensure accurate comparisons, control tests were conducted with the optimal $BiVO_4$ thin film in the absence of light, as well as uncoated glass in both light and dark conditions. There was a reduction in the concentration of *E. coli* over time, from a high initial inoculum reaching values lower than the method's limit of detection (<LD) within 48 h (Figure 7a). In the presence of light, the superoxide radical ($O_2^{-\bullet}$) formed - as described in topic 3.2.3 - reacts with hydrogen to form hydrogen peroxide (H_2O_2) [84,85]. The concentration gradient generated due to hydrogen peroxide causes cell disruption, deformation, and disorganization [86]. Furthermore, in the dark control tests, there was

an antimicrobial activity of $BiOV_4$, reaching values <LD within 72 h (Figure 7b), suggesting some innate antimicrobial action. The average result after 24 h in the light and 48h in the dark had a major associated error because the value was very close to the LD, there was no growth in some samples.

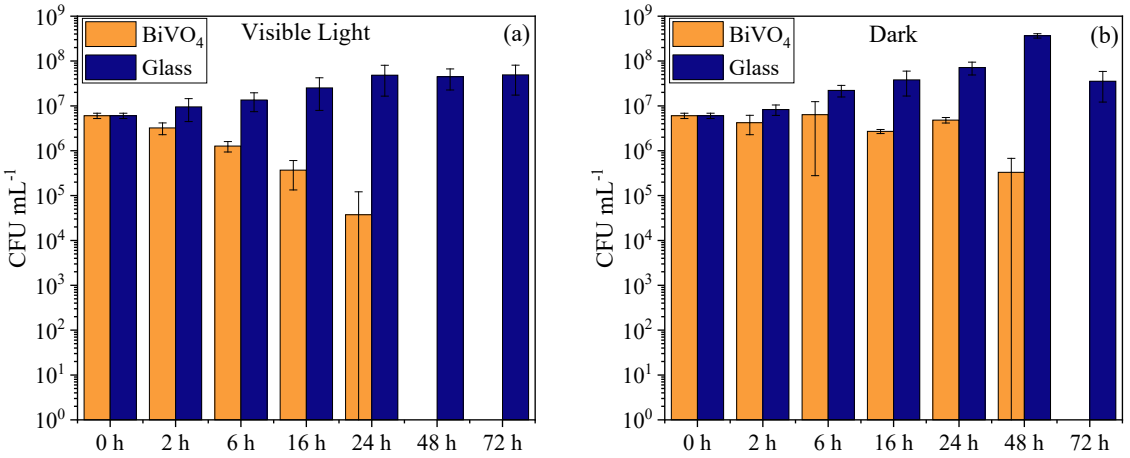

Figure 7. Number of microbial cells (CFU mL^{-1}) recovered from the samples of glass and $BiVO_4$ thin films, until 72 h, (a) irradiated with the visible light; and (b) in the dark. Data represents triplicate samples which were repeated twice.

Ratova et al. [30] assessed the antimicrobial activity of bismuth tungstate (Bi_2WO_4), bismuth oxide (BiO), and titanium dioxide (TiO_2) thin films produced by magnetron sputtering under visible light. Values <LD just were achieved after 48 h with BiO, whilst Bi_2WO_4 after 72 h and TiO_2 did not reach concentrations <LD in 72 h tested. Sharma et al. [78] reported the inactivation of *E. coli* by monoclinic $BiVO_4$ powder of 96% within 2 h with a photocatalyst concentration of 80 ppm under visible light illumination, where almost 100% degradation was achieved after 8 h. Ekthammathat et al. [77] by synthesizing $BiVO_4$ powder through the hydrothermal method, had no antimicrobial activity in tests with *E. coli*, only a reduction in concentration in tests with *S. aureus*. Xiang et al. [48] synthesizing β-$AgVO_3$/$BiVO_4$ powder by hydrothermal method, achieved values <LD of *P. aeruginosa* under visible light. It is worth noting that none of these or other studies report any antimicrobial activity of the $BiVO_4$ in the dark; on the contrary, in the absence of light, the works reported inactivity.

A number of investigations have demonstrated the antimicrobial activity of bismuth-based compounds under different light sources [88–90]. Outside of applications in

492 photocatalysis and water treatment, bismuth has been employed as an antimicrobial agent
493 in pharmaceutical compounds. The interaction between bismuth and other antimicrobial
494 agents can be enhanced by coordination, as exemplified by bismuth conjugates with
495 fluoroquinolone, including norfloxacin and ciprofloxacin [91,92]. In the same way, other
496 antimicrobial applications of vanadium-based compounds have been investigated [93–
497 95]. The antimicrobial activity of both compounds separately, and in different
498 applications, adds to the previously unparalleled results obtained in the field of
499 photocatalysis and water treatment suggests new possibilities for a safe drinking water
500 disinfection.

501 *3.4 BiVO4 cytotoxicity assessment*

502 The different concentrations of $BiVO_4$ that the cells were exposed to result in different
503 effects, ranging from non-toxic to strongly cytotoxic according to ISO 10993–5 (Figure
504 8). From the concentrations tested, up to 10 ppm resulted in nontoxic. In concentrations
505 of 25 and 50 mg L^{-1}, the material starts to show some toxicity to the CACO-2 cells, being
506 considered weakly cytotoxic and reaching moderate toxicity at 100 mg L^{-1}. The maximum
507 toxicity level was achieved at 250 mg L^{-1} of the material, falling under strongly cytotoxic.
508 An unexpected behavior was observed which was confirmed by the repetition in the
509 biological replicates, the reduction in cytotoxicity with the increase in concentration from
510 250 mg L^{-1}. Thus, the cells exposed to 500 and 1000 mg L^{-1} were considered to be
511 moderately cytotoxic. This may result from the particles becoming entangled within the
512 cells as they grow and not being removed during the wash phase. Any additional
513 absorbance from $BiVO_4$ may appear as absorbance from cells and thus increase the cell
514 viability %.

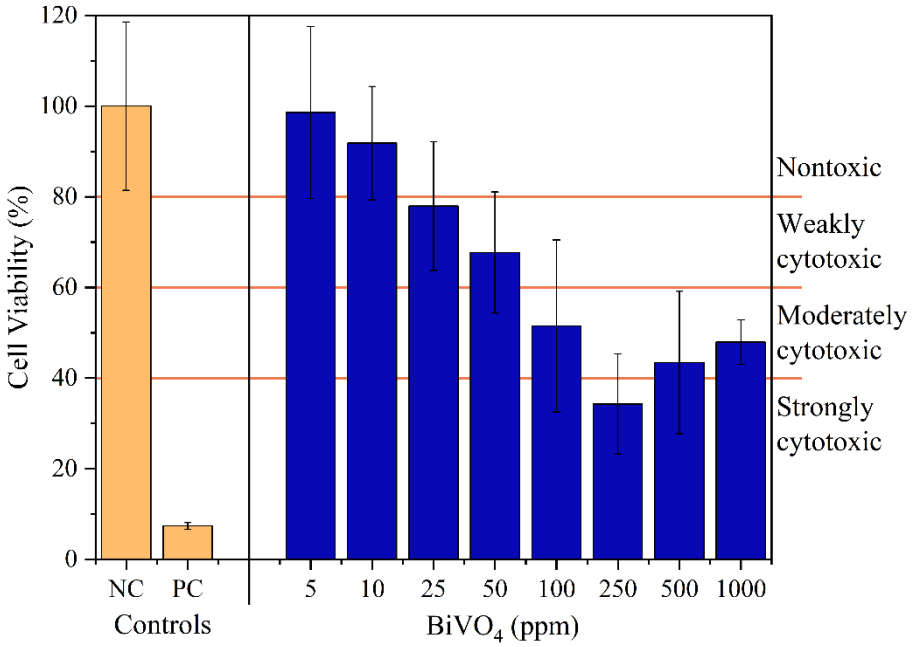

Figure 8. Viability of CACO-2 cells in the cytotoxic test of $BiVO_4$ at concentrations ranging from 5 to 1000 ppm with its negative (NC) and positive (PC) controls according to ISO 10993–5.

Same papers tested the $BiVO_4$ cytotoxicity with different cells, Mohamed et al. [87] with human rhabdomyosarcoma cells and human laryngeal carcinoma cells and Ghotekar et al. [88] with a breast cancer cell line. They achieved strong toxicity with concentrations up to 125 mg L^{-1}; a similar result as found in the present work. It is important to note the distinction between this and those works that have been applied in film form, which makes it safer to apply to water treatment. The TEM images of the optimal $BiVO_4$ immediately after production, and this film, after both antimicrobial and 15 consecutive cycles of MB degradation tests, provides valuable insights (Figure 8). When comparing these three situations, no significant differences were observed. The $BiVO_4$ thin film is therefore safe to use in water treatment, as it remains stable throughout the treatment cycles. There was no evidence that the material had been taken away, which would have allowed it to be ingested with the treated water. This further supports the need to advance the techniques for producing and applying photocatalytic thin films with a view to treating drinking water.

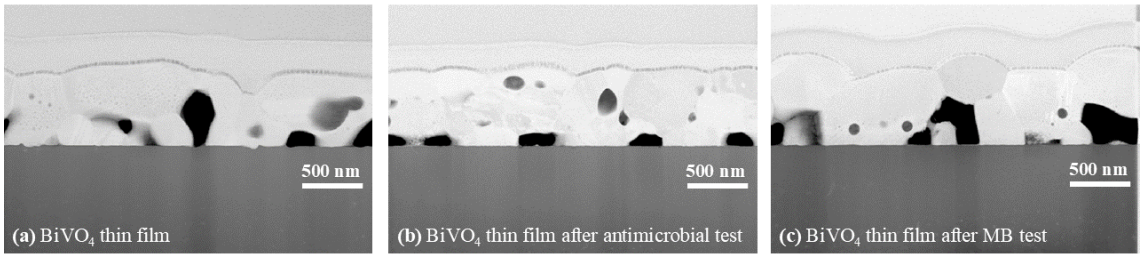

Figure 9. TEM images of the (a) optimal $BiVO_4$ thin film, (b) optimal $BiVO_4$ thin film after the antimicrobial test, and (c) optimal $BiVO_4$ thin film after 15 consecutive cycles.

3. CONCLUSION

The bottom line is that the use of a design of experiments tool, such as the Taguchi method, proved crucial in identifying the best operating conditions for producing thin films via magnetron sputtering for water treatment. However, it is important to emphasize that more robust experimental designs can be employed to achieve a more refined adjustment of the tested factors and levels, as well as to better account for interactions and non-linearities. Therefore, this stage was essential to obtain functional films that effectively fulfill their intended purpose. Based on the evaluated factors and levels, the optimal conditions for producing thin $BiVO_4$ films for water treatment under visible light were determined to be a pressure of 4 mTorr, a pulse frequency of 100 kHz, a 90% duty cycle, and a deposition time of 2 h. Films produced under these conditions exhibited antimicrobial activity under both light and dark conditions and demonstrated high photocatalytic stability across multiple cycles.

The observed antimicrobial activity is unprecedented and represents a significant opportunity for advancements in the field of disinfection. Such developments could provide a safer alternative to conventional drinking water treatment methods, which have been associated with health risks due to disinfection by-products from chlorine. The prospect of further investigations is eagerly anticipated, as the implementation of the photocatalytic process in real-life water treatment is full of various complex challenges. To that end, it is recommended that future research incorporate this photocatalytic thin film into scalable reactors, thereby facilitating its application. It is imperative to acknowledge the numerous challenges that must be addressed for this application to be realized, including the reaction temperatures, the complexity of bacterial species, variable

pH values, and the interactions of other elements. Achieving breakthroughs in alternative disinfection methods has the potential to catalyze the formulation of public policies that aim to redirect the field by establishing new legal guidelines.

Acknowledgements

The Coordenação de Aperfeiçoamento de Pessoal de Nível Superior – Brasil (CAPES) in for international mobility scholarship under the CAPES-PRINT program (001; process n. 88887.803016/2023-00); the foundation of Support and Research of the state of Minas Gerais (FAPEMIG) [153357703 ID:73]; and the National Council for Scientific and Technological Development (CNPq) [314642/2021 8] have supported this work. Funding sources were not involved in study design, nor the collection, analysis, and interpretation of data, nor in the writing of the report, nor in the decision to submit the paper to this journal.

4. REFERENCES

[1] United Nations (UN), Clean Water and Sanitation, (2023).

[2] World Health Organization (WHO), Guidelines for drinking-water quality, 4th ed., 2017.

[3] A. Rodríguez-Otero, N. Losada-García, S. Guerra-Rodríguez, J.M. Palomo, J. Rodríguez-Chueca, Antibacterial effect of metal-enzyme hybrid nanomaterials, J Environ Chem Eng 11 (2023) 110499. https://doi.org/10.1016/j.jece.2023.110499.

[4] M.A. Mazhar, N.A. Khan, S. Ahmed, A.H. Khan, A. Hussain, Rahisuddin, F. Changani, M. Yousefi, S. Ahmadi, V. Vambol, Chlorination disinfection by-products in municipal drinking water – A review, J Clean Prod 273 (2020) 123159. https://doi.org/10.1016/j.jclepro.2020.123159.

586 [5] X. Lei, Y. Lei, X. Zhang, X. Yang, Treating disinfection byproducts with UV or
587 solar irradiation and in UV advanced oxidation processes: A review, J Hazard
588 Mater 408 (2021) 124435. https://doi.org/10.1016/j.jhazmat.2020.124435.

589 [6] G.C.C. Viana, E.M.R. Rocha, E. Scapin, A. Cahino, I.R.D. Leite, D.A. Bertuol,
590 J.D. Ardisson, D.A.S. Rodrigues, C.C. Amorim, Solar photocatalysis using post-
591 consumer alkaline batteries for degrading contaminants of emerging concern in
592 surface water, J Environ Chem Eng 11 (2023) 111226.
593 https://doi.org/10.1016/j.jece.2023.111226.

594 [7] M.C.V.M. Starling, C.C. Amorim, M.M.D. Leão, Occurrence, control and fate of
595 contaminants of emerging concern in environmental compartments in Brazil, J
596 Hazard Mater (2019) 17–36. https://doi.org/10.1016/j.jhazmat.2018.04.043.

597 [8] S. Younis, K.-H. Kim, Heterogeneous Photocatalysis Scalability for
598 Environmental Remediation: Opportunities and Challenges, Catalysts 10 (2020)
599 1109. https://doi.org/10.3390/catal10101109.

600 [9] H. Dong, G. Zeng, L. Tang, C. Fan, C. Zhang, X. He, Y. He, An overview on
601 limitations of TiO2-based particles for photocatalytic degradation of organic
602 pollutants and the corresponding countermeasures, Water Res 79 (2015) 128–146.
603 https://doi.org/10.1016/j.watres.2015.04.038.

604 [10] J. Du, S. Xu, Q. Zhou, H. Li, L. Fu, J.-H. Tang, M.-Q. Jin, The ecotoxicology of
605 titanium dioxide nanoparticles, an important engineering nanomaterial, Toxicol
606 Environ Chem 101 (2019) 165–189.
607 https://doi.org/10.1080/02772248.2019.1693572.

608 [11] R.B.P. Marcelino, C.C. Amorim, M. Ratova, B. Delfour-Peyrethon, P. Kelly,
609 Novel and versatile TiO2 thin films on PET for photocatalytic removal of
610 contaminants of emerging concern from water, Chemical Engineering Journal 370
611 (2019) 1251–1261. https://doi.org/10.1016/j.cej.2019.03.284.

612 [12] I. Grčić, N. Koprivanac, G. Li Puma, Modeling the photocatalytic oxidation of
613 carboxylic acids on aqueous TiO2 suspensions and on immobilized TiO2-chitosan
614 thin films in different reactor geometries irradiated by UVA or UVC light sources,

615 Chemical Engineering Journal 422 (2021) 130104.
616 https://doi.org/10.1016/j.cej.2021.130104.

617 [13] R.S. Pedanekar, S.K. Shaikh, K.Y. Rajpure, Thin film photocatalysis for
618 environmental remediation: A status review, Current Applied Physics 20 (2020)
619 931–952. https://doi.org/10.1016/j.cap.2020.04.006.

620 [14] A. Di Mauro, M.E. Fragalà, V. Privitera, G. Impellizzeri, ZnO for application in
621 photocatalysis: From thin films to nanostructures, Mater Sci Semicond Process 69
622 (2017) 44–51. https://doi.org/https://doi.org/10.1016/j.mssp.2017.03.029.

623 [15] M. Grao, M. Ratova, C.C. Amorim, R.B.P. Marcelino, P. Kelly, Crystalline TiO2
624 supported on stainless steel mesh deposited in a one step process via pulsed DC
625 magnetron sputtering for wastewater treatment applications, Journal of Materials
626 Research and Technology 9 (2020) 5761–5773.
627 https://doi.org/10.1016/j.jmrt.2020.03.101.

628 [16] M. Ratova, R. Marcelino, P. de Souza, C. Amorim, P. Kelly, Reactive Magnetron
629 Sputter Deposition of Bismuth Tungstate Coatings for Water Treatment
630 Applications under Natural Sunlight, Catalysts 7 (2017) 283.
631 https://doi.org/10.3390/catal7100283.

632 [17] J. Redfern, M. Ratova, A.P. Dean, J. Pritchett, M. Grao, J. Verran, P. Kelly, Visible
633 light photocatalytic bismuth oxide coatings are effective at suppressing aquatic
634 cyanobacteria and degrading free-floating genomic DNA, J Environ Sci (China)
635 104 (2021) 128–136. https://doi.org/10.1016/j.jes.2020.11.024.

636 [18] A. Scimone, J. Redfern, P. Patiphatpanya, T. Thongtem, M. Ratova, P. Kelly, J.
637 Verran, Development of a rapid method for assessing the efficacy of antibacterial
638 photocatalytic coatings, Talanta 225 (2021).
639 https://doi.org/10.1016/j.talanta.2020.122009.

640 [19] P.R. Dutra, C.C. Amorim, P.L. Gastelois, M. Grao, M. Ratova, A.P. Santos, P.
641 Kelly, Carbonaceous-TiO2 composite photocatalysts through reactive direct
642 current magnetron sputtering on powdered graphene for environmental
643 applications, Thin Solid Films 792 (2024) 140248.
644 https://doi.org/10.1016/j.tsf.2024.140248.

[20] P.J. Kelly, R.D. Arnell, Magnetron sputtering: a review of recent developments and applications, Vacuum 56 (2000) 159–172. https://doi.org/10.1016/S0042-207X(99)00189-X.

[21] R. Garg, S. Gonuguntla, S. Sk, M.S. Iqbal, A.O. Dada, U. Pal, M. Ahmadipour, Sputtering thin films: Materials, applications, challenges and future directions, Adv Colloid Interface Sci 330 (2024) 103203. https://doi.org/10.1016/j.cis.2024.103203.

[22] T. Nimalan, M.R. Begam, Physical and Chemical Methods: A Review on the Analysis of Deposition Parameters of Thin Film Preparation Methods, International Journal of Thin Film Science and Technology 13 (2024) 59–66. https://doi.org/10.18576/ijtfst/130107.

[23] S.K. Padamata, A. Yasinskiy, V. Yanov, G. Saevarsdottir, Magnetron Sputtering High-Entropy Alloy Coatings: A Mini-Review, Metals (Basel) 12 (2022) 319. https://doi.org/10.3390/met12020319.

[24] O.K. Alexeeva, V.N. Fateev, Application of the magnetron sputtering for nanostructured electrocatalysts synthesis, Int J Hydrogen Energy 41 (2016) 3373–3386. https://doi.org/10.1016/j.ijhydene.2015.12.147.

[25] X.-Q. Tan, J.-Y. Liu, J.-R. Niu, J.-Y. Liu, J.-Y. Tian, Recent Progress in Magnetron Sputtering Technology Used on Fabrics, Materials 11 (2018) 1953. https://doi.org/10.3390/ma11101953.

[26] M. Pálmai, E.M. Zahran, S. Angaramo, S. Bálint, Z. Pászti, M.R. Knecht, L.G. Bachas, Pd-decorated m-$BiVO_4$/BiOBr ternary composite with dual heterojunction for enhanced photocatalytic activity, J Mater Chem A Mater 5 (2017) 529–534. https://doi.org/10.1039/C6TA08357A.

[27] L. Chen, D. Meng, X. Wu, A. Wang, J. Wang, M. Yu, Y. Liang, Enhanced visible light photocatalytic performances of self-assembled hierarchically structured $BiVO_4$/Bi_2WO_6 heterojunction composites with different morphologies, RSC Adv 6 (2016) 52300–52309. https://doi.org/10.1039/C6RA08685C.

673 [28] H. Huang, L. Liu, Y. Zhang, N. Tian, Novel BiIO $_4$ /BiVO $_4$ composite
674 photocatalyst with highly improved visible-light-induced photocatalytic
675 performance for rhodamine B degradation and photocurrent generation, RSC Adv
676 5 (2015) 1161–1167. https://doi.org/10.1039/C4RA12916D.

677 [29] T. Fan, C. Chen, Z. Tang, Hydrothermal synthesis of novel BiFeO $_3$ /BiVO $_4$
678 heterojunctions with enhanced photocatalytic activities under visible light
679 irradiation, RSC Adv 6 (2016) 9994–10000.
680 https://doi.org/10.1039/C5RA26500B.

681 [30] M. Shang, W. Wang, J. Ren, S. Sun, L. Zhang, A novel BiVO4 hierarchical
682 nanostructure: controllable synthesis, growth mechanism, and application in
683 photocatalysis, CrystEngComm 12 (2010) 1754.
684 https://doi.org/10.1039/b923115c.

685 [31] M. Grao, J. Redfern, P. Kelly, M. Ratova, Photocatalytic degradation of
686 contaminants of emerging concern using a low-cost and efficient black bismuth
687 titanate-based water treatment reactor, Journal of Water Process Engineering 45
688 (2022). https://doi.org/10.1016/j.jwpe.2021.102525.

689 [32] M. Ratova, J. Redfern, J. Verran, P.J. Kelly, Highly efficient photocatalytic
690 bismuth oxide coatings and their antimicrobial properties under visible light
691 irradiation, Appl Catal B 239 (2018) 223–232.
692 https://doi.org/10.1016/j.apcatb.2018.08.020.

693 [33] D. Lv, D. Zhang, X. Pu, D. Kong, Z. Lu, X. Shao, H. Ma, J. Dou, One-pot
694 combustion synthesis of BiVO4/BiOCl composites with enhanced visible-light
695 photocatalytic properties, Sep Purif Technol 174 (2017) 97–103.
696 https://doi.org/10.1016/j.seppur.2016.10.010.

697 [34] Y. Hu, J. Fan, C. Pu, H. Li, E. Liu, X. Hu, Facile synthesis of double cone-shaped
698 Ag4V2O7/BiVO4 nanocomposites with enhanced visible light photocatalytic
699 activity for environmental purification, J Photochem Photobiol A Chem 337
700 (2017) 172–183. https://doi.org/10.1016/j.jphotochem.2016.12.035.

[35] L. Ye, L. Tian, T. Peng, L. Zan, Synthesis of highly symmetrical BiOI single-crystal nanosheets and their {001} facet-dependent photoactivity, J Mater Chem 21 (2011) 12479. https://doi.org/10.1039/c1jm11005e.

[36] Y. Feng, C. Liu, J. Chen, H. Che, L. Xiao, W. Gu, W. Shi, Facile synthesis of BiOI/CdWO 4 p–n junctions: enhanced photocatalytic activities and photoelectrochemistry, RSC Adv 6 (2016) 38290–38299. https://doi.org/10.1039/C5RA23383F.

[37] M.F.R. Samsudin, S. Sufian, B.H. Hameed, Epigrammatic progress and perspective on the photocatalytic properties of BiVO4-based photocatalyst in photocatalytic water treatment technology: A review, J Mol Liq 268 (2018) 438–459. https://doi.org/10.1016/j.molliq.2018.07.051.

[38] L. Chen, J. He, Y. Liu, P. Chen, C.-T. Au, S.-F. Yin, Recent advances in bismuth-containing photocatalysts with heterojunctions, Chinese Journal of Catalysis 37 (2016) 780–791. https://doi.org/10.1016/S1872-2067(15)61061-0.

[39] Z.-F. Huang, L. Pan, J.-J. Zou, X. Zhang, L. Wang, Nanostructured bismuth vanadate-based materials for solar-energy-driven water oxidation: a review on recent progress, Nanoscale 6 (2014) 14044–14063. https://doi.org/10.1039/C4NR05245E.

[40] A. Malathi, J. Madhavan, M. Ashokkumar, P. Arunachalam, A review on BiVO 4 photocatalyst: Activity enhancement methods for solar photocatalytic applications, Appl Catal A Gen 555 (2018) 47–74. https://doi.org/10.1016/j.apcata.2018.02.010.

[41] V.I. Merupo, S. Velumani, G. Oza, M. Tabellout, M. Bizarro, S. Coste, A.H. Kassiba, High Energy Ball-Milling Synthesis of Nanostructured Ag-Doped and BiVO 4 -Based Photocatalysts, ChemistrySelect 1 (2016) 1278–1286. https://doi.org/10.1002/slct.201600090.

[42] M. Wang, C. Niu, J. Liu, Q. Wang, C. Yang, H. Zheng, Effective visible light-active nitrogen and samarium co-doped BiVO4 for the degradation of organic pollutants, J Alloys Compd 648 (2015) 1109–1115. https://doi.org/10.1016/j.jallcom.2015.05.115.

730 [43] S. Dong, J. Feng, Y. Li, L. Hu, M. Liu, Y. Wang, Y. Pi, J. Sun, J. Sun, Shape-
731 controlled synthesis of BiVO4 hierarchical structures with unique natural-sunlight-
732 driven photocatalytic activity, Appl Catal B 152–153 (2014) 413–424.
733 https://doi.org/10.1016/j.apcatb.2014.01.059.

734 [44] R. Venkatesan, S. Velumani, K. Ordon, M. Makowska-Janusik, G. Corbel, A.
735 Kassiba, Nanostructured bismuth vanadate (BiVO4) thin films for efficient visible
736 light photocatalysis, Mater Chem Phys 205 (2018) 325–333.
737 https://doi.org/10.1016/j.matchemphys.2017.11.004.

738 [45] C.R. Dhas, D. Arivukarasan, R. Venkatesh, A.J. Josephine, K.C.M. Gnana Malar,
739 S.E. Santhoshi Monica, B. Subramanian, Influence of precursor aging time period
740 on physical and photocatalytic properties of nebulizer spray coated BiVO4 thin
741 films, Solid State Sci 92 (2019) 36–45.
742 https://doi.org/10.1016/j.solidstatesciences.2019.04.006.

743 [46] N. Kiama, C. Ponchio, Photoelectrocatalytic performance improvement of BiVO4
744 thin film fabrication via effecting of calcination temperature strategy, Surf Coat
745 Technol 383 (2020) 125257. https://doi.org/10.1016/j.surfcoat.2019.125257.

746 [47] S. Bakhtiarnia, S. Sheibani, A. Billard, H. Sun, E. Aubry, M.A.P. Yazdi, Enhanced
747 photocatalytic activity of sputter-deposited nanoporous BiVO4 thin films by
748 controlling film thickness, J Alloys Compd 879 (2021) 160463.
749 https://doi.org/10.1016/j.jallcom.2021.160463.

750 [48] S. Bakhtiarnia, S. Sheibani, A. Nadi, E. Aubry, H. Sun, P. Briois, M.A.P. Yazdi,
751 Preparation of sputter-deposited Cu-doped BiVO4 nanoporous thin films
752 comprised of amorphous/crystalline heterostructure as enhanced visible-light
753 photocatalyst, Appl Surf Sci 608 (2023) 155248.
754 https://doi.org/10.1016/j.apsusc.2022.155248.

755 [49] S.K. Holland, M.R. Dutter, D.J. Lawrence, B.A. Reisner, T.C. DeVore,
756 Photoelectrochemical performance of W-doped BiVO4 thin films deposited by
757 spray pyrolysis, J Photonics Energy 4 (2014) 041598.
758 https://doi.org/10.1117/1.JPE.4.041598.

[50] Z. Xiang, Y. Wang, Z. Yang, D. Zhang, Heterojunctions of β-AgVO3/BiVO4 composites for enhanced visible-light-driven photocatalytic antibacterial activity, J Alloys Compd 776 (2019) 266–275. https://doi.org/10.1016/j.jallcom.2018.10.287.

[51] Y. Zhang, Z. Yi, G. Wu, Q. Shen, Novel Y doped BiVO4 thin film electrodes for enhanced photoelectric and photocatalytic performance, J Photochem Photobiol A Chem 327 (2016) 25–32. https://doi.org/10.1016/j.jphotochem.2016.05.004.

[52] M.W. Hisam, A.A. Dar, M.O. Elrasheed, M.S. Khan, R. Gera, I. Azad, The Versatility of the Taguchi Method: Optimizing Experiments Across Diverse Disciplines, Journal of Statistical Theory and Applications 23 (2024) 365–389. https://doi.org/10.1007/s44199-024-00093-9.

[53] J. Tauc, Optical properties and electronic structure of amorphous Ge and Si, Mater Res Bull 3 (1968) 37–46. https://doi.org/10.1016/0025-5408(68)90023-8.

[54] J. Liang, Y. Wei, Y. Yao, X. Zheng, J. Shen, G. He, H. Chen, Constructing high-efficiency photocatalyst for degrading ciprofloxacin: Three-dimensional visible light driven graphene based NiAlFe LDH, J Colloid Interface Sci 540 (2019) 237–246. https://doi.org/10.1016/j.jcis.2019.01.011.

[55] Q. Liu, Y. Guo, Z. Chen, Z. Zhang, X. Fang, Constructing a novel ternary Fe(III)/graphene/g-C 3 N 4 composite photocatalyst with enhanced visible-light driven photocatalytic activity via interfacial charge transfer effect, Appl Catal B 183 (2016) 231–241. https://doi.org/10.1016/j.apcatb.2015.10.054.

[56] W. Zhao, Y. Feng, H. Huang, P. Zhou, J. Li, L. Zhang, B. Dai, J. Xu, F. Zhu, N. Sheng, D.Y.C. Leung, A novel Z-scheme Ag3VO4/BiVO4 heterojunction photocatalyst: Study on the excellent photocatalytic performance and photocatalytic mechanism, Appl Catal B 245 (2019) 448–458. https://doi.org/10.1016/j.apcatb.2019.01.001.

[57] R. Gupta, B. Boruah, J.M. Modak, G. Madras, Kinetic study of Z-scheme C3N4/CuWO4 photocatalyst towards solar light inactivation of mixed populated bacteria, J Photochem Photobiol A Chem 372 (2019) 108–121. https://doi.org/10.1016/j.jphotochem.2018.08.035.

[58] K. Ding, W. Wang, D. Yu, W. Wang, P. Gao, B. Liu, Facile formation of flexible Ag/AgCl/polydopamine/cotton fabric composite photocatalysts as an efficient visible-light photocatalysts, Appl Surf Sci 454 (2018) 101–111. https://doi.org/10.1016/j.apsusc.2018.05.154.

[59] N. Liu, Q. Zhu, N. Zhang, C. Zhang, N. Kawazoe, G. Chen, N. Negishi, Y. Yang, Superior disinfection effect of Escherichia coli by hydrothermal synthesized TiO2-based composite photocatalyst under LED irradiation: Influence of environmental factors and disinfection mechanism, Environmental Pollution 247 (2019) 847–856. https://doi.org/10.1016/j.envpol.2019.01.082.

[60] W. Deng, H. Zhao, F. Pan, X. Feng, B. Jung, A. Abdel-Wahab, B. Batchelor, Y. Li, Visible-Light-Driven Photocatalytic Degradation of Organic Water Pollutants Promoted by Sulfite Addition, Environ Sci Technol 51 (2017) 13372–13379. https://doi.org/10.1021/acs.est.7b04206.

[61] C.-L. Chang, S.-G. Shih, P.-H. Chen, W.-C. Chen, C.-T. Ho, W.-Y. Wu, Effect of duty cycles on the deposition and characteristics of high power impulse magnetron sputtering deposited TiN thin films, Surf Coat Technol 259 (2014) 232–237. https://doi.org/10.1016/j.surfcoat.2014.03.011.

[62] K. Sarakinos, J. Alami, S. Konstantinidis, High power pulsed magnetron sputtering: A review on scientific and engineering state of the art, Surf Coat Technol 204 (2010) 1661–1684. https://doi.org/10.1016/j.surfcoat.2009.11.013.

[63] Q. Lu, L. Ding, J. Li, N. Wang, M. Ji, N. Wang, K. Chang, High transmittance BiVO4 thin-film photoanodes by reactive magnetron sputtering for a photovoltaic-photoelectrocatalysis water splitting system, Int J Hydrogen Energy 71 (2024) 1142–1150. https://doi.org/10.1016/j.ijhydene.2024.04.168.

[64] S. Wang, T. He, P. Chen, A. Du, K. (Ken) Ostrikov, W. Huang, L. Wang, Water Splitting: In Situ Formation of Oxygen Vacancies Achieving Near-Complete Charge Separation in Planar $BiVO_4$ Photoanodes (Adv. Mater. 26/2020), Advanced Materials 32 (2020). https://doi.org/10.1002/adma.202070198.

[65] L. Zhang, M. Zhao, Y. Chen, H. Chen, F. Wang, L. Ma, H. Ma, Effect of sputtering pressure on the electrochromic properties of flexible NiO films prepared by

819 magnetron sputtering, Mater Lett 354 (2024) 135317.
820 https://doi.org/10.1016/j.matlet.2023.135317.

821 [66] W. Lee, S.-W. Lee, S. Bae, J.-K. Hwang, Y. Kim, S.-H. Jeong, J.-S. Hwang, S.
822 Lee, D. Kim, Y. Kang, H.-S. Lee, Unraveling the effect of working pressure on the
823 morphological, structural, optical, and compositional properties of PbI2 thin films
824 deposited by RF magnetron sputtering, Appl Surf Sci 684 (2025) 161888.
825 https://doi.org/10.1016/j.apsusc.2024.161888.

826 [67] R. Garg, S. Gonuguntla, S. Sk, M.S. Iqbal, A.O. Dada, U. Pal, M. Ahmadipour,
827 Sputtering thin films: Materials, applications, challenges and future directions,
828 Adv Colloid Interface Sci 330 (2024) 103203.
829 https://doi.org/10.1016/j.cis.2024.103203.

830 [68] J.J. Rueda-Marquez, I. Levchuk, P. Fernández Ibañez, M. Sillanpää, A critical
831 review on application of photocatalysis for toxicity reduction of real wastewaters,
832 J Clean Prod 258 (2020) 120694. https://doi.org/10.1016/j.jclepro.2020.120694.

833 [69] H. Khan, A.S. Yerramilli, A. D'Oliveira, T.L. Alford, D.C. Boffito, G.S. Patience,
834 Experimental methods in chemical engineering: X-ray diffraction spectroscopy—
835 <scp>XRD</scp>, Can J Chem Eng 98 (2020) 1255–1266.
836 https://doi.org/10.1002/cjce.23747.

837 [70] B. Guan, J. Chen, Z. Li, Z. Zhuang, Y. Chen, Z. Ma, J. Guo, C. Zhu, X. Hu, S.
838 Zhao, H. Dang, L. Chen, K. Shu, Z. Guo, K. Shi, Y. Li, C. Yi, J. Hu, Z. Huang,
839 Review on Synthesis, Modification, Morphology, and Combination of $BiVO_4$ -
840 based Catalysts for Photochemistry: Status, Advances, and Perspectives, Energy
841 & Fuels 38 (2024) 806–853. https://doi.org/10.1021/acs.energyfuels.3c03932.

842 [71] L. Zhang, Z. Chen, H. Ma, Effect of sputtering pressure and oxygen content on the
843 electrochromic properties of NiO films by DC magnetron sputtering, Physica B
844 Condens Matter 677 (2024) 415663. https://doi.org/10.1016/j.physb.2024.415663.

845 [72] M. Grao, J. Redfern, P.J. Kelly, M. Ratova, Magnetron co-sputtered
846 Bi12TiO20/Bi4Ti3O12 composite – An efficient photocatalytic material with
847 photoinduced oxygen vacancies for water treatment application, Appl Surf Sci 552
848 (2021) 149486. https://doi.org/10.1016/j.apsusc.2021.149486.

[73] Z. Guo, Y. Mao, Optimization of Ga2O3 thin film growth via magnetron sputtering: Influence of growth pressure on crystallinity, surface morphology, and optical properties, Vacuum 234 (2025) 114057. https://doi.org/10.1016/j.vacuum.2025.114057.

[74] K. Ćwik, J. Zawadzki, R. Zybała, M. Ożga, B. Witkowski, P. Wojnar, M. Wolska-Pietkiewicz, M. Jędrzejewska, J. Lewiński, M.A. Borysiewicz, Magnetron Sputtering as a Solvent-Free Method for Fabrication of Nanoporous ZnO Thin Films for Highly Efficient Photocatalytic Organic Pollution Degradation, Compounds 4 (2024) 534–547. https://doi.org/10.3390/compounds4030032.

[75] K. Tolod, S. Hernández, N. Russo, Recent Advances in the BiVO4 Photocatalyst for Sun-Driven Water Oxidation: Top-Performing Photoanodes and Scale-Up Challenges, Catalysts 7 (2017) 13. https://doi.org/10.3390/catal7010013.

[76] O. Monfort, G. Plesch, Bismuth vanadate-based semiconductor photocatalysts: a short critical review on the efficiency and the mechanism of photodegradation of organic pollutants, Environmental Science and Pollution Research 25 (2018) 19362–19379. https://doi.org/10.1007/s11356-018-2437-9.

[77] J. Gan, X. Lu, Y. Tong, Towards highly efficient photoanodes: boosting sunlight-driven semiconductor nanomaterials for water oxidation, Nanoscale 6 (2014) 7142. https://doi.org/10.1039/c4nr01181c.

[78] Y. Zhang, G. Li, Recent Advances of Epitaxial BiVO4 Thin Film: Preparation and Physical and Photoelectrochemical Properties, Brazilian Journal of Physics 50 (2020) 185–191. https://doi.org/10.1007/s13538-019-00730-0.

[79] H. Yoon, M.G. Mali, H.Y. Kim, S.S. Al-Deyab, S.S. Yoon, Efficient Water Purification by Photocatalysis and Rapid Adsorption of Dip-Coated Metal Foam with Nanostructured Bismuth Vanadate, Journal of the American Ceramic Society 99 (2016) 1023–1030. https://doi.org/10.1111/jace.13993.

[80] J.L. Lopes, A.C. Estrada, S. Fateixa, N.A. Sobolev, A.L. Daniel-da-Silva, T. Trindade, Visible-light activation of carbon-supported BiVO4 photocatalysts, J Photochem Photobiol A Chem 447 (2024) 115174. https://doi.org/10.1016/j.jphotochem.2023.115174.

[81] M. A., M. J., M. Ashokkumar, P. Arunachalam, A review on BiVO 4 photocatalyst: Activity enhancement methods for solar photocatalytic applications, Appl Catal A Gen 555 (2018) 47–74. https://doi.org/10.1016/j.apcata.2018.02.010.

[82] M. Wang, P. Guo, T. Chai, Y. Xie, J. Han, M. You, Y. Wang, T. Zhu, Effects of Cu dopants on the structures and photocatalytic performance of cocoon-like Cu-BiVO4 prepared via ethylene glycol solvothermal method, J Alloys Compd 691 (2017) 8–14. https://doi.org/10.1016/j.jallcom.2016.08.198.

[83] R. Andreozzi, Advanced oxidation processes (AOP) for water purification and recovery, Catal Today 53 (1999) 51–59. https://doi.org/10.1016/S0920-5861(99)00102-9.

[84] N.A. Khan, S.U. Khan, S. Ahmed, I.H. Farooqi, A. Dhingra, A. Hussain, F. Changani, Applications of Nanotechnology in Water and Wastewater Treatment: A Review, Asian Journal of Water, Environment and Pollution 16 (2019) 81–86. https://doi.org/10.3233/AJW190051.

[85] M.N. Chong, B. Jin, C.W.K. Chow, C. Saint, Recent developments in photocatalytic water treatment technology: A review, Water Res 44 (2010) 2997–3027. https://doi.org/10.1016/j.watres.2010.02.039.

[86] N. Ekthammathat, A. Phuruangrat, S. Thongtem, T. Thongtem, Synthesis, Characterization and Antibacterial Activity of BiVO4 Microstructure, Russian Journal of Physical Chemistry A 92 (2018) 1036–1040. https://doi.org/10.1134/S0036024418050114.

[87] R. Sharma, Uma, S. Singh, A. Verma, M. Khanuja, Visible light induced bactericidal and photocatalytic activity of hydrothermally synthesized BiVO 4 nano-octahedrals, J Photochem Photobiol B 162 (2016) 266–272. https://doi.org/10.1016/j.jphotobiol.2016.06.035.

[88] Q. Sun, M. Ke, Y. Zhao, B. Wang, J. Zhang, J. Sheng, Embellishing {0 0 1} surface of Bi2MoO6 nanobelts with enhanced photocatalytic performance and mechanisms exploration, Appl Surf Sci 563 (2021) 150104. https://doi.org/10.1016/j.apsusc.2021.150104.

[89] M. Karbasi, F. Karimzadeh, K. Raeissi, S. Rtimi, J. Kiwi, S. Giannakis, C. Pulgarin, Insights into the Photocatalytic Bacterial Inactivation by Flower-Like Bi2WO6 under Solar or Visible Light, Through in Situ Monitoring and Determination of Reactive Oxygen Species (ROS), Water (Basel) 12 (2020) 1099. https://doi.org/10.3390/w12041099.

[90] V. Subhiksha, S. Kokilavani, S. Sudheer Khan, Recent advances in degradation of organic pollutant in aqueous solutions using bismuth based photocatalysts: A review, Chemosphere 290 (2022) 133228. https://doi.org/10.1016/j.chemosphere.2021.133228.

[91] R. Wang, H. Li, H. Sun, Bismuth: Environmental Pollution and Health Effects, in: Encyclopedia of Environmental Health, Elsevier, 2019: pp. 415–423. https://doi.org/10.1016/B978-0-12-409548-9.11870-6.

[92] R. Wang, T.-P. Lai, P. Gao, H. Zhang, P.-L. Ho, P.C.-Y. Woo, G. Ma, R.Y.-T. Kao, H. Li, H. Sun, Bismuth antimicrobial drugs serve as broad-spectrum metallo-β-lactamase inhibitors, Nat Commun 9 (2018) 439. https://doi.org/10.1038/s41467-018-02828-6.

[93] J. Wang, H. Zhou, G. Guo, T. Cheng, X. Peng, X. Mao, J. Li, X. Zhang, A functionalized surface modification with vanadium nanoparticles of various valences against implant-associated bloodstream infection, Int J Nanomedicine Volume 12 (2017) 3121–3136. https://doi.org/10.2147/IJN.S129459.

[94] C. Sridhar, N. Gunvanthrao Yernale, M.V.N.A. Prasad, Synthesis, Spectral Characterization, and Antibacterial and Antifungal Studies of PANI/V_2O_5 Nanocomposites, International Journal of Chemical Engineering 2016 (2016) 1–6. https://doi.org/10.1155/2016/3479248.

[95] A.A. Sharfalddin, I.M. Al-Younis, H.A. Mohammed, M. Dhahri, F. Mouffouk, H. Abu Ali, Md.J. Anwar, K.A. Qureshi, M.A. Hussien, M. Alghrably, M. Jaremko, N. Alasmael, J.I. Lachowicz, A.-H. Emwas, Therapeutic Properties of Vanadium Complexes, Inorganics (Basel) 10 (2022) 244. https://doi.org/10.3390/inorganics10120244.

[96] H.E.A. Mohamed, S. Afridi, A.T. Khalil, T. Zohra, M.M. Alam, A. Ikram, Z.K. Shinwari, M. Maaza, Phytosynthesis of BiVo4 nanorods using hyphaene thebaica for diverse biomedical applications, AMB Express 9 (2019). https://doi.org/10.1186/s13568-019-0923-1.

[97] S. Ghotekar, S.R. Mishra, M. Ahmaruzzaman, P. Basnet, K.Y.A. Lin, A. Rahdar, R. Oza, A novel eco-benevolent synthesis of BiVO4 nanoparticles using cow urine for antioxidant, anticancer, and photocatalytic activities, Biomass Convers Biorefin (2023). https://doi.org/10.1007/s13399-023-05015-w.